Molecular modeling and assessment of cytotoxic and apoptotic potentials of imatinib analogues featuring (thio)urea motifs in human leukemia and lymphoma cells

Özlem BİNGÖL ÖZAKPINAR [1] (ID), **Aslı TÜRE [2] *** (ID), **İlkay KÜÇÜKGÜZEL [2]** (ID)

[1]   Department of Biochemistry, Faculty of Pharmacy, Marmara University, Haydarpaşa 34668 İstanbul, Turkey.
[2]   Department of Pharmaceutical Chemistry, Faculty of Pharmacy, Marmara University, Haydarpaşa 34668 İstanbul, Turkey.
*   Corresponding Author. E-mail: asli.demirci@marmara.edu.tr (A.T.); Tel. +90-216-414 29 63.

ABSTRACT: Imatinib is a well-known anticancer drug. In this study, cytotoxic properties of thirty-two imatinib analogues featuring (thio)urea motifs have been evaluated against chronic myeloid leukemia (K562), Burkitt lymphoma (Raji) and mouse embryonic fibroblast (NIH 3T3) cells. IC_{50} values of selected eleven compounds were calculated against K562 and NIH 3T3 cells. Apoptotic properties of the most active three compounds were evaluated on K652 cells subsequently. Favorably, compounds **19**, **31** and **32** induced early apoptotic changes on K562 cells. Loss of membrane potential as well as caspase-3 and caspase-9 activation was determined in the present study. Levels of anti-apoptotic proteins, Bcl-XL and Bcl-2 decreased after the implementation of compounds **19**, **31** and **32** at 10 μM and 50 μM concentrations. To reveal further molecular insight into the anticancer activity of the compounds, compounds **19**, **31** and **32** were docked into ABL kinase protein as imatinib shows anticancer activity by inhibiting this enzyme. Modeling studies demonstrated significant molecular interactions between compounds **19**, **31** and **32** and ABL protein. Compounds **19**, **31** and **32** showed excellent superposition with imatinib in the binding site of ABL. These findings suggest that compounds **19**, **31** and **32** have potential to show anticancer activity against chronic myeloid leukemia.

KEYWORDS: Imatinib analogues; ABL kinase; chronic myeloid leukemia; lymphoma; molecular modeling; docking.

1. INTRODUCTION

Cancer is set to become the major malignant health disorder in the following decades. It threatens millions of lives worldwide. The global cancer burden is growing day by day. Today, one in six deaths are from cancer, one in five people are predicted to develop cancer during their lifetime [1]. More than 200 different types of cancer have been identified until now [2] and a wide range of anticancer drugs is used to treat various cancers in the clinic [3]. Among the drugs that are used to treat cancer, imatinib stands out to be the first molecule discovered by rational drug design approaches. Imatinib is the first-line anticancer therapy for the treatment of chronic myeloid leukemia (CML) and also it was approved for the treatment of hematoproliferative neoplasms (e.g., CML, acute lymphoblastic leukemia (ALL), chronic eosinophilic leukemia, chronic myelomonocytic leukemia), as well as gastrointestinal stromal cancer. Imatinib is the pioneering protein kinase inhibitor and has been used in the clinic for years in the CML therapy. It owes its clinical success to the inhibition of ABL kinase protein [4-6].

Cancer cells differentiate from healthy cells with diverse functions. Twenty years ago, Hanahan and Weinberg defined certain cancer cell capabilities as "*Hallmarks of Cancer*". These hallmarks include sustained angiogenesis, limitless replicative potential, tissue invasion and metastasis, insensitivity to anti-growth signals and evading apoptosis [7]. A great amount of effort in the field of anti-cancer drug discovery has been made to understand the mechanisms underlying hallmarks of cancer and to overcome these cancer cell functions as well. Over activation of kinase proteins is considered one of the distinctive properties of cancer cells. The human genome comprises 538 kinases. Overactivation of different kinase proteins is linked with different cancers [8,9]. It is well known that overexpression of ABL kinase by the induction of v-ABL or BCR-ABL causes CML [10]. As indicated above, another hallmark of cancer cells is the reduced apoptotic functions [7]. In this concept, investigation of apoptotic properties of potential anticancer drugs becomes substantial.

In our previous study, the cytotoxic profile of thirty-two imatinib analogues featuring (thio)urea motifs **1-32** was evaluated on colon (HCT116), breast (MCF-7) and liver (Huh7) cancer cell lines and selected compounds were evaluated against liver carcinoma panel. Cell cycle analysis and apoptosis studies were held on liver carcinoma cells (Huh7 and Mahlavu) additionally [11]. Since compounds **1-32** are imatinib analogues and imatinib is used to treat CML in the clinic, we were enthusiastically curious about the anticancer activities of these compounds on CML cells. In another study of ours, imatinib analogues containing 1,3- thiazolidin-4-one ring were screened against CML and we provided promising results [12]. Based on these starting points, we evaluated anticancer of the compounds **1-32** on K562 (CML) and Raji (Burkitt lymphoma) in the present study. Cytotoxicity of compounds **1-32** was also evaluated on NIH 3T3 (mouse embryonic fibroblast) cells. Proliferation percentage of the cells and IC_{50} values of the compounds were determined subsequently. Compounds, which exhibited better cytotoxicity results, were selected for further studies. Apoptosis studies including Annexin V staining, measurement of caspase activation, analysis of Bcl-c and Bcl-XL proteins and detection of the loss of mitochondrial membrane potential was screened. Possible ABL kinase inhibition properties of the compounds were visualized by the help of molecular docking implementations.

2. RESULTS AND DISCUSSION

2.1. Biological studies

Before biological studies, chemical structures of thirty-two (thio)urea motif derived imatinib analogues were enlightened extensively and published in our previous report [11]. Compounds were initially tested for their anticancer activity on K562 and Raji cells. While viability of Raji cells was found between %103.88 and %58.49, cell viability of K562 cells was found between %91.29 and %58.79 at 10 μM. Compounds are found to be more cytotoxic against K562 cells in general. Cytotoxic profile of these compounds was also evaluated on NIH 3T3 cells and cell proliferation of NIH 3T3 cells was found between %119.60 and %66.21. Cell viability assessment was performed compared to imatinib and results are presented in Table 1. Compound **31** showed the most inhibitory activity on K562 cells with %58.79 cell proliferation and compound **19** showed the most inhibitory activity on Raji cells %58.49 cell proliferation. Out of thirty-two, eleven compounds (**15**, **16**, **17**, **18**, **19**, **20**, **22**, **25**, **28**, **31** and **32**) were selected to be tested for their IC_{50} values on K562 and NIH 3T3 cells (Table 2) and three compounds (**19**, **31** and **32**) were selected for the follow-up apoptosis studies. Chemical structures of compounds **19**, **31** and **32** along with imatinib is shown in Figure 1. IC_{50} values of the selected compounds **19**, **31** and **32** were found to be 13.14 μM, 19.44 μM and 14.75 μM respectively against K562 cells. Additionally, against NIH 3T3 cells, IC_{50} values of the compounds **19**, **31** and **32** were found to be 82.48 μM, 84.34 μM and 87.74 μM respectively. Thus, cytotoxicity of compounds **19**, **31** and **32** against NIH 3T3 cells was found less than cytotoxicity of the compounds against K562 cells.

Many anticancer strategies are based on the enhancement of apoptosis in cancer cells as a means to shrink tumors. From this perspective, apoptotic profile of the compounds **19**, **31** and **32** on K562 cells was subsequently evaluated by Annexin V binding assay, measurement of caspase activation, measurement of Bcl-2 and Bcl-XL activity and detection of the loss of mitochondrial membrane potential studies. In the early stages of apoptosis, cellular changes occur in the cell surface. In healthy cells, phosphatidylserine (PS), an anionic phospholipid, is confined in the inner membrane leaflet. The translocation of PS to the outer leaflet is an early event in apoptosis and it serves as a signal for the attack of phagocytic cells. The released PS can be detected by Annexin V binding. Annexin V discriminates apoptotic and non-apoptotic cells via flow cytometric assay method [13]. In our study, compounds **19**, **31** and **32** initiated early apoptotic processes in K562 cells according to the results of Annexin V staining assay (Figure 2).

The caspase family of proteases initiates and executes apoptotic cell death. Members of caspase family are divided into two sub-families as initiator caspases that are activated in the first instance and executioner caspases that are activated in the final stages. While caspase-2, -8, -9 and -10 are initiator caspases; caspase-3, -6, and -7 are known as executioner caspase proteins [14]. In this study, executioner caspase-3 and initiator caspase-9 activation after the implementation of compounds **19**, **31** and **32** at 10 μM and 50 μM concentrations was evaluated on K562 cells. Studies showed that caspase-3 activity folded 3-5 times and caspase-9 activity folded 2-4 times compared to control after treatment of compounds **19**, **31** and **32** at 10 μM and 50 μM concentrations (Figure 3). Consequently, compounds induced apoptosis through caspase-3 and caspase-9 dependent pathways. It was observed that caspase-3 and caspase-9 activity increased in dose dependent manner and compound **32** showed the best caspase-3 and caspase-9 pathway activation up to 5 times at 50 μM concentration.

As mitochondrial morphology changes during apoptosis, mitochondrial structure alterations are identified to have crucial roles in apoptotic processes. Detection loss of mitochondrial membrane potential is recognized as an apoptotic marker [15]. In this concept, detection of the loss of mitochondrial membrane potential was studied and it was observed that compounds **19**, **31** and **32** induced the loss of mitochondrial membrane potential in the K562 cells at 10 μM and 50 μM concentrations (Figure 4).

Bcl-2 and Bcl-XL proteins are known as anti-apoptotic proteins [16]. After the implementation of compounds **19**, **31** and **32** at 10 μM and 50 μM concentrations, levels of anti-apoptotic proteins Bcl-2 and Bcl-XL reduced in K562 cells (Figure 5).

Table 1. Percentage viability values of the compounds **1-32**.

Compound	X	R	%Cell proliferation		
			Raji	K562	NIH 3T3
1	S	-H	103.88	88.37	119.60
2	S	methyl	102.64	86.86	94.79
3	S	ethyl	84.65	82.50	126.76
4	S	propyl	90.50	88.75	112.57
5	S	allyl	88.10	86.40	109.05
6	S	butyl	79.81	86.33	81.58
7	S	cyclohexyl	82.67	84.39	95.38
8	S	4-morpholinoethyl	84.30	87.84	86.07
9	S	benzyl	89.69	91.29	66.21
10	S	4-chlorophenethyl	73.95	80.42	111.13
11	S	phenyl	79.77	84.09	91.93
12	S	4-fluorophenyl	85.04	86.89	112.96
13	S	4-chlorophenyl	82.95	85.53	103.84
14	S	5-chloro-2-methylphenyl	69.69	80.00	105.60
15	S	2,4-dichlorophenyl	63.45	77.84	101.37
16	S	3-trifluoromethylphenyl	59.88	73.71	98.50
17	S	4-trifluoromethylphenyl	62.56	77.39	105.01
18	S	2-chloro-5-trifluoromethylphenyl	60.74	74.43	96.55
19	S	4-chloro-3-trifluoromethylphenyl	58.49	64.36	90.82
20	S	3,5-bis-(trifluoromethyl)phenyl	65.19	82.16	106.77
21	S	4-trifluoromethoxyphenyl	68.37	78.37	83.46
22	S	4-nitrophenyl	65.47	75.19	78.84
23	S	benzoyl	78.80	78.79	82.94
24	S	4-methoxybenzoyl	82.33	84.28	94.14
25	S	4-chlorobenzoyl	85.23	66.14	80.79
26	S	4-nitrobenzoyl	78.68	77.39	94.21
27	S	4-bromobenzoyl	74.46	85.37	104.95
28	O	4-chlorophenyl	63.57	75.49	81.71
29	O	4-trifluoromethylphenyl	71.94	67.69	70.70
30	O	3-trifluoromethylphenyl	70.00	83.86	75.59
31	O	4-fluoro-3-trifluoromethylphenyl	75.62	58.79	86.65
32	O	3,5-bis-(trifluoromethyl)phenyl	65.27	63.14	72.40
Imatinib	-	-	56.65	60.46	148.83
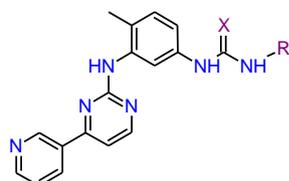
Table 2. IC$_{50}$ results of the most active compounds.

Compound	IC$_{50}$ (µM)	
	K562	NIH 3T3
15	66.34	90.31
16	51.48	94.14
17	82.77	104.71
18	35.75	87.06
19	13.14	82.48
20	54.66	75.33
22	35.02	95.02
25	72.17	102.34
28	52.43	79.31
31	19.44	84.34
32	14.75	87.74
Imatinib	7.16	>300
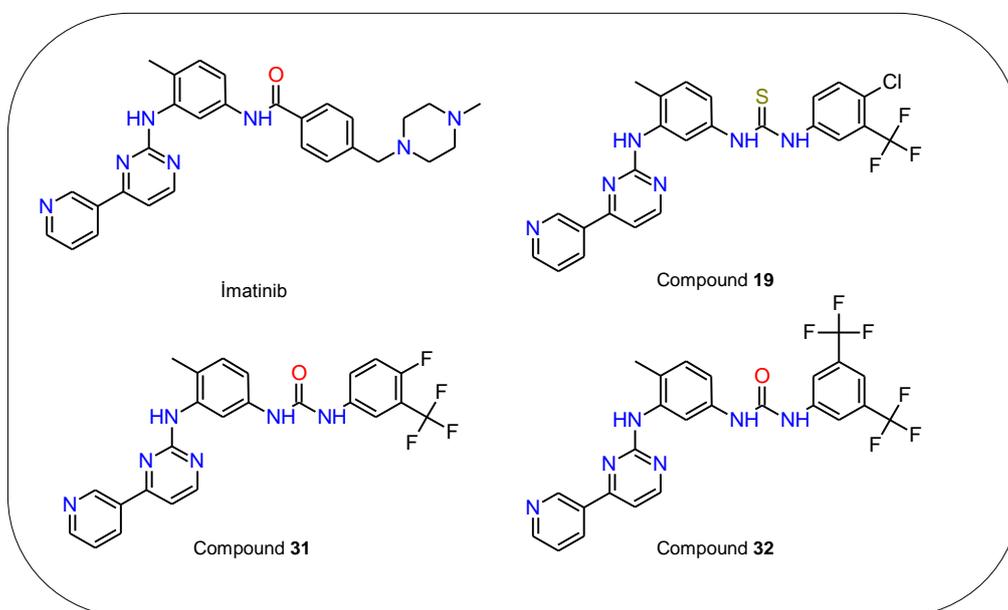
Figure 1. 2D structures of the most active compounds **19**, **31**, **32** and imatinib.
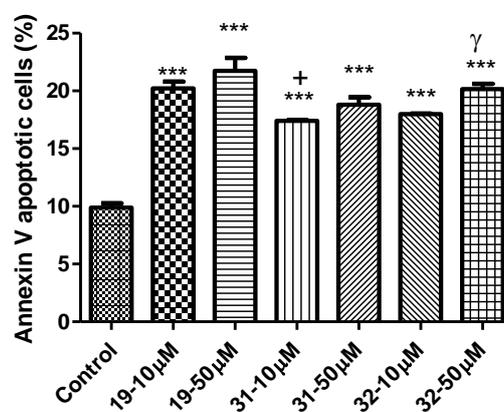
Figure 2. Early apoptotic effects of compounds **19**, **31** and **32** on K562 cells at 10 µM and 50 µM concentrations (Results are presented as mean ± SD, statistically significant differences are expressed ***$p < 0.001$ vs control; *$p < 0.5$ vs compounds-10 µM; $^{\Upsilon}p < 0.05$ vs compounds-50 µM).
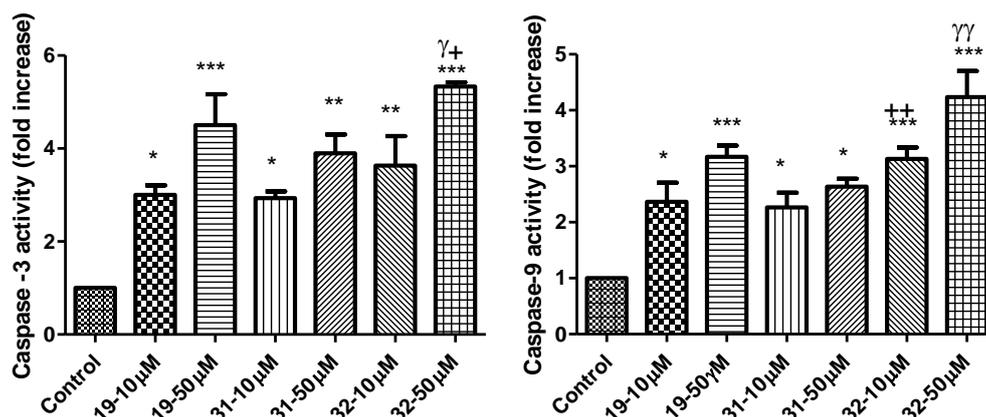
Figure 3. Caspase-3 and caspase-9 activation of K562 cells after treatment of compounds **19**, **31** and **32** at 10 μM and 50 μM concentrations (Results are presented as mean ± SD, statistically significant differences are expressed *$p < 0.5$, **$p < 0.01$ and ***$p < 0.001$ vs control; +$p<0.05$ and ++$p<0.01$ vs compounds-10 μM; $^{Y}p<0.05$ and $^{YY}p<0.01$ vs compounds-50 μM.).
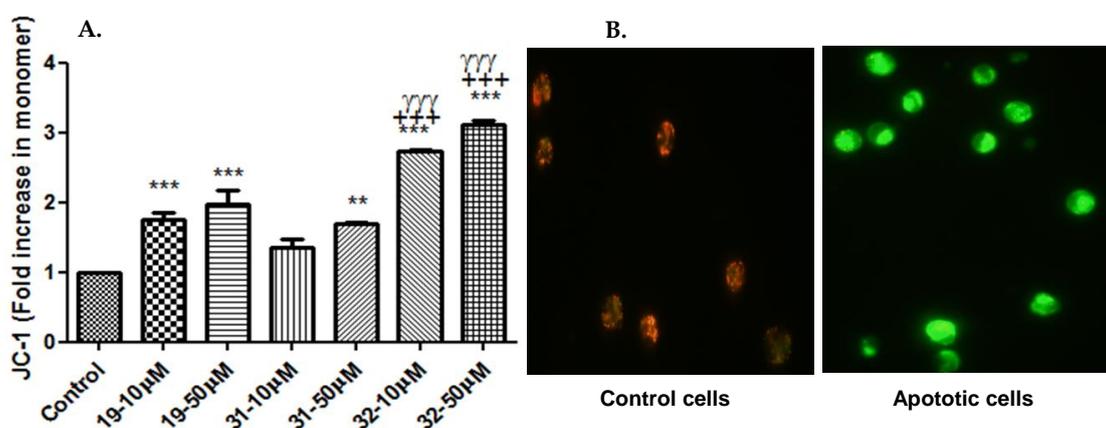
Figure 4. A. Effects of compounds **19**, **31** and **32** at 10 μM and 50 μM concentrations on mitochondrial membrane potential in K562 cells (Results are presented as mean ± SD, statistically significant differences are expressed as **$p < 0.01$, ***$p < 0.001$ vs control; +++$p<0,001$ vs Compound 19-10 μM; $^{YYY}p<0.001$ vs Compound 19-50 μM). **B.** Representative images show JC-1 fluorescence in control and treated K562 cells incubated with compound **32** at 50 μM concentration.
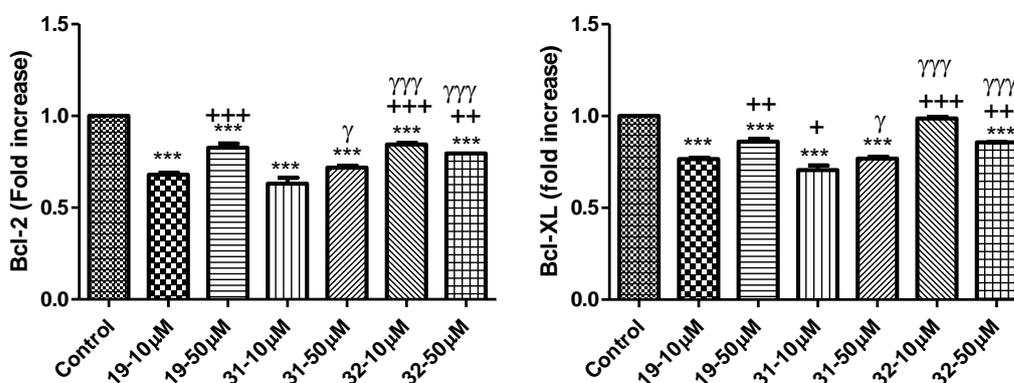
Figure 5. Effects of compounds **19**, **31** and **32** at 10 μM and 50 μM concentrations on Bcl-2 and Bcl-XL in K562 cells (Results are presented as mean ± SD, statistically significant differences are expressed ***$p < 0.001$ vs control; +$p<0.05$, ++$p<0,01$ and +++$p<0,001$ vs compounds-10 μM; $^{Y}p<0.05$ and $^{YYY}p<0.001$ vs compounds-50 μM).

It is noteworthy that among the compounds **1-32**, compound **19** was found as one of the most active compounds against Huh7, MCF7 and HCT116 cells with IC_{50} values of 4.6 μM, 4.9 μM and 7.9 μM respectively and it was selected for further studies in our previous research [11].

While designing imatinib analogs, we were inspired with the chemical structure of sorafenib, which is a very well-known urea derivative protein kinase inhibitor used to treat hepatocellular carcinoma, renal cell carcinoma and differentiated thyroid cancer [17-19], so that we introduced urea and thiourea motifs to the structure of phenylaminopyrimidine core of imatinib. In particular, compound **19** was designed with a hybrid approach as it contains 4-chloro-3-trifluoromethylphenyl substituent in the structure likewise sorafenib does [20]. A more detailed analysis of the binding interactions of 4-chloro-3-trifluoromethylphenyl substituent is discussed in the following section named *in silico* studies. It was also noticed that all the most active compounds have 3-trifluoromethylphenyl substituents in their structures as can be seen in Figure 1. Trifluoromethyl group locates in a fundamental position of active compounds and enhances biological activity. In the medicinal chemistry platform, fluorinated organic compounds has reached the deserved reputation owing to electron withdrawing properties and greater stabilities as well as greater lipophilicities [21]. In this respect, we were expecting to observe better activity of fluorinated compounds.

2.2. *In silico* studies

To put further molecular insight into the anticancer activity of the compounds, docking studies were held meanwhile. Overactivation of ABL kinase has been demonstrated to be linked with CML and inhibition of the activity of ABL kinase could be an effective strategy to fight with CML [22]. ABL kinase is also a well-known anti-apoptotic protein [23]. Inhibiting ABL activity with ligands, cell survival decreases and programmed cell death called apoptosis elevates (Figure 6). In this study, possible inhibition mechanisms of ABL kinase by compounds **19**, **31** and **32** as ligands was investigated.
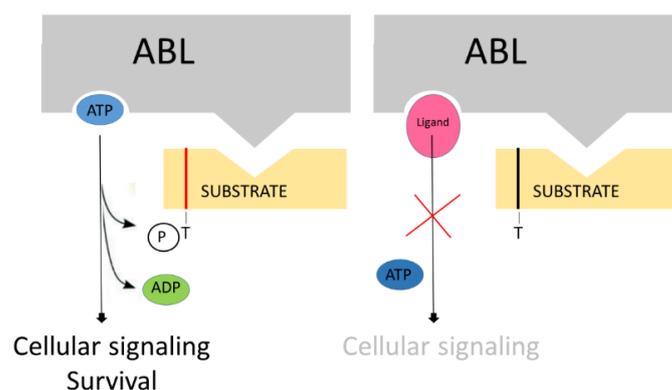

Figure 6. Inhibition of ABL activity results in decreased cell functions.

Molecular modeling studies were run with DFG (single letter abbreviations of Aspartic acid, Phenyl alanine and Glutamic acid) out inactive state of ABL kinase. Docking conformations of compounds **19**, **31** and **32** showed favorable superposition between phenylaminopyrimidine cores of designed (thio)urea analogues and imatinib (Figure 7) and possible binding conformation of each ligand was evaluated one by one. Interactions with the hinge region, especially interactions with Met318 residue, interactions with gatekeeper residue Thr315 and interactions with DFG motif of the kinase proteins which are both crucial for kinase inhibition were visualized after docking processes.

According to the docking calculations, nitrogen atom in pyridine ring of compound **19** makes hydrogen bond interaction with Met318. Thiourea hydrogen atoms make hydrogen bond interactions with Glu286 of DFG motif. NH atom of phenylaminopyrimidine group interacts with oxygen atom of gatekeeper Thr315 forming hydrogen bond. Chlorine substituent of 4-chloro-3-trifluoromethylphenyl ring perfectly settles in the hydrophobic pocket and makes hydrophobic interactions desirably. Fluorine atoms of 4-chloro-3-trifluoromethylphenyl ring makes halogen interactions with His361. Pi-anion interaction between phenyl ring of chloro-3-trifluoromethylphenyl substitution and Asp381 amino acid of DFG motif is visualized. T shaped pi-pi stacked interactions is observed between pyrimidine ring and Tyr253. Pi-sigma interactions are detected between pyridine ring and Leu248 and Leu370. Alkyl and pi-alkyl interactions are formed with Val256, Ala269, Lys271, Met290, Val289, Leu354 and Phe359 amino acid residues of activation site (Figure 8).
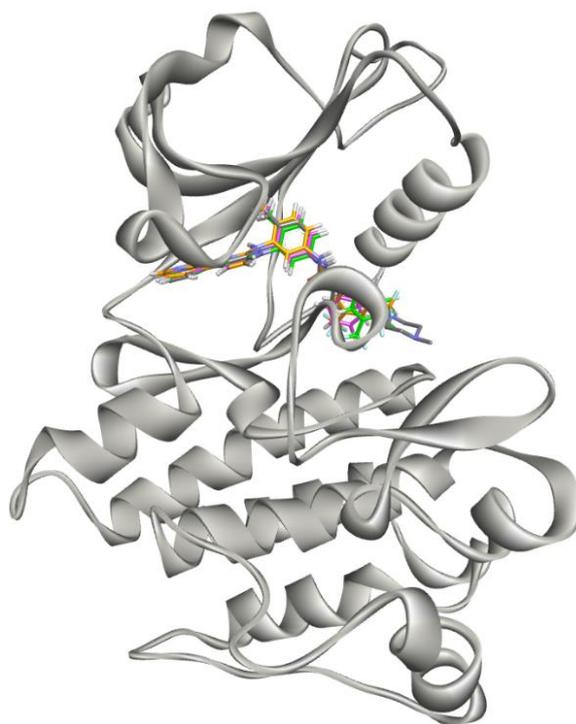
Figure 7. 3D x-ray structure of ABL kinase with ligands. As ABL kinase protein is depicted as white ribbon, imatinib molecule which is co-crystallized with ABL kinase is shown grey sticks. Docked conformations of compounds **19**, **31** and **32** are presented as orange, pink and green sticks respectively.
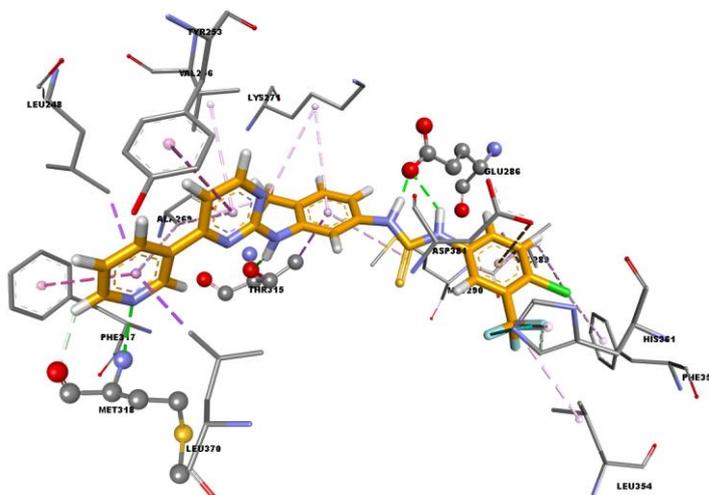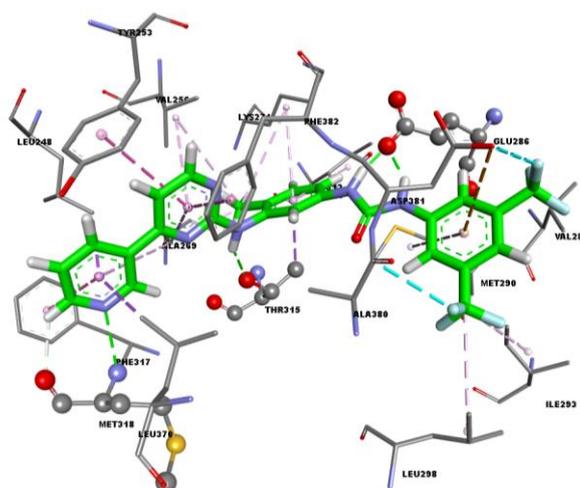

Figure 8. Molecular interactions between Compound **19** and ABL kinase. Compound **19** is depicted orange in its stick form. While amino acid residues in the activation site of ABL is presented with sticks; Glu286, Thr315 and Met318 amino acid residues, which form H bond interaction with compound **19**, are presented as ball-stick.

Results of the docking calculation of compound **31** showed that nitrogen atom in pyridine ring forms hydrogen bond interaction with Met318. As thiourea hydrogen atoms make hydrogen bond interactions with Glu286 residue of DFG motif, thiourea S atom forms hydrogen bond interaction with Asp381 residue of DFG motif. NH group of phenylaminopyrimidine group acts as hydrogen bond donor and interacts hydrogen bond with the gatekeeper Thr315. 3-Trifluoromethyl group of 4-fluoro-3-trifluoromethylphenyl ring makes halogen interactions with Ile360. Pi-sigma interactions are visualized between pyridine ring and Leu248 and Leu370 as well as phenyl ring and Thr315. While pi-pi interactions are detected with Tyr253, Phe317 and Phe382, alkyl interactions are observed with Val256, Ala269, Lys271 and Ile313 amino acid residues (Figure 9).
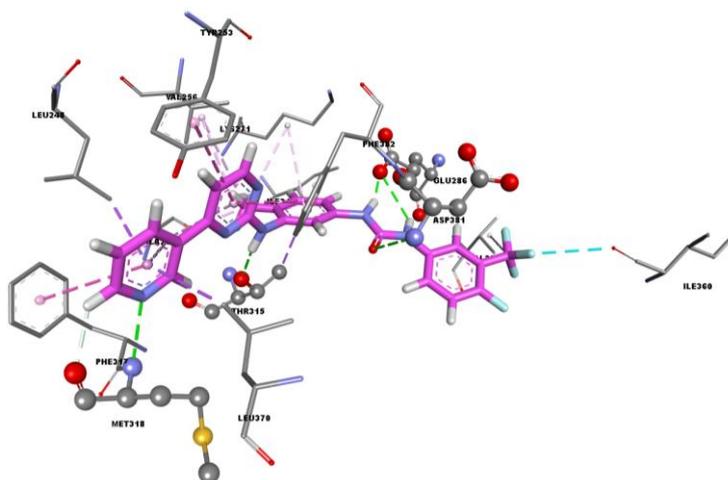
Figure 9. Molecular interactions between Compound **31** and ABL kinase. Compound **31** is depicted pink in its stick form. While amino acid residues in the activation site of ABL is presented with sticks; Glu286, Thr315, Met318 and Asp381 amino acid residues, which form H bond interaction with compound **31**, are presented as ball-stick.

Docking calculations with compound **32** indicated that nitrogen atom in pyridine ring forms hydrogen bond interaction with Met318 amino acid residue of the hinge region. Thiourea hydrogen atoms make hydrogen bond interactions with Glu286 residue of DFG motif. NH group of phenylaminopyrimidine group forms hydrogen bond interaction with the gatekeeper Thr315 playing as hydrogen bond donor. 3-Trifluoromethyl groups of 3,5-bis-trifluoromethylphenyl ring form halogen interactions with Ala380 and Asp381. Pi-anion interactions are detected between phenyl ring of 3,5-bis-trifluoromethylphenyl substituent and Asp381 amino acid of DFG motif. Alkyl and pi-alkyl interactions are observed with Val256, Ala269, Lys271, Val289, Met290, Ile293, Leu298 and Ile313 amino acids (Figure 10).

Figure 10. Molecular interactions between Compound **32** and ABL kinase. Compound **31** is depicted green in its stick form. While amino acid residues in the activation site of ABL is presented with sticks; Glu286, Thr315 and Met318 and amino acid residues, which form H bond interaction with compound **32**, are presented as ball-stick.

3. CONCLUSION

Cytotoxic activity and apoptotic profile of compounds **1-32** was evaluated in the current study. Compounds **1-32** showed moderate toxicity against K562 and Raji cells. IC$_{50}$ values of eleven compounds showing better cytotoxicity were calculated and three compounds **19**, **31** and **32** possessing IC$_{50}$ values of 13.14 µM, 19.44 µM and 14.75 µM respectively against K562 cells were selected for the continued studies. Follow-up studies were implemented with K562 cells. Apoptotic profile of compounds **19**, **31** and **32** was evaluated with Annexin V staining assay, measurement of caspase-3 and caspase-9 activation, measurement of Bcl-2 and Bcl-XL protein levels and detection of the loss of mitochondrial membrane potential studies.

Annexin V staining assay indicated that early apoptotic processes start after the treatment of compounds **19**, **31** and **32**. Compounds **19**, **31** and **32** induced a spectacularly significant increase in caspase-3 up to 3-5 and caspase-9 activity up to 2-4 fold in dose-dependent manner. Levels of well-known anti-apoptotic proteins Bcl-2 and Bcl-XL decreased after the implementation of these compounds. Loss of mitochondrial membrane potential was observed in dose-dependent manner as well.

To reveal further molecular insight into the activity of the imatinib analogues, docking calculations were held with ABL kinase protein based on the link between CML and over activation of ABL kinase. Remarkable molecular interactions were observed between compounds **19**, **31** and **32** and ABL kinase. In the light of docking studies, imatinib analogues **19**, **31** and **32** are predicted to be ABL inhibitors.

In conclusion, three (thio)urea derived imatinib analogues **19**, **31** and **32** was shown to be apoptotic agents and possible ABL inhibitors.

4. MATERIALS AND METHODS

4.1. Biological studies

4.1.1. Cell culture studies

Human chronic myeloid leukemia cell line (K562), human Burkitt's lymphoma cell line (Raji) and non-tumorigenic mouse embryonic fibroblast cell line (NIH 3T3) were purchased from American Type Culture Collection (ATCC) (Manassas, VA, USA). Cells were cultured in Dulbecco's modified eagle medium (DMEM) (Gibco, Rockville, MD, USA) containing 10% fetal bovine serum (FBS) (Gibco, Rockville, MD, USA) and maintained in a 37°C, 5% CO_2 incubator. Cell passage was conducted at 80-90% confluence.

4.1.2. Cell viability assay

Cell viability was determined by the 3-(4,5-dimethylthiazol-2-yl)-2,5-diphenyltetrazolium bromide (MTT) assay. In brief, K562, Raji and NIH 3T3 cells (1×10^4 cells/well) were seeded onto 96-well plates and incubated overnight. Subsequently, cells were treated with 10 µM of compounds for 48 h. MTT was added into each well to a final concentration of 0.5 mg/mL and cell were incubated for 4 h afterwards. After culture medium was removed, 100 µL of the SDS buffer was added to solubilize the purple formazan product. Absorbance of plates at 570 and 630 nm wavelength were measured by a microplate reader (Biotek, Winooski, VT, USA).

4.1.3. Apoptosis studies

Annexin V binding

Following the treatment, cells were centrifuged and resuspended in cold PBS afterwards. After incubation of cells with annexin V for 15 min at room temperature in the dark. Then, cells were washed and centrifuged at 1000 x g for 5 min at room temperature. The cell pellet gently was resuspend in 0.5 ml cold 1X binding buffer and added 10 µl Propidium Iodide. Fuorescence intensity was measured using a fluorescence Elisa reader.

Measurement of caspase-3 and caspase-9 activation

Caspase activation was determined using colorimetric assay kits (Millipore) following the manufacturer's protocol. Following the treatment, cells were lysed in ice-cold lysis buffer. Samples were centrifuged at 10,000 x g for 1 min. Subsequently, the supernatants were collected and the protein concentrations were measured by the Bradford method. Samples containing 200 µg protein were incubated with 5 µl of the 4mM p-nitroanilide (pNA) substrates, (DEVD-pNA for caspase-3 and LEHD-pNA for caspase-9) for 2 h at 37°C. pNA cleavage was observed spectrophotometrically using an EPOCH microplate reader (Biotek, Winooski, VT, USA) at 405 nm. Data are expressed as fold increase in caspase activity.

Measurement of Bcl-2 and Bcl-XL activity

Cells were permeabilized in Cytofix/Cytoperm buffer (BD Biosciences, USA) for cytoplasmic staining with a fluorescein isothiocyanate (FITC)-conjugated monoclonal mouse antihuman Bcl-2 and Bcl-XL antibody (DAKO, Glostrup, Denmark). The samples were incubated with Bcl-2 and Bcl-XL antibodies seperately for 30 minutes at room temperature. Next, cells were washed and resuspended in wash buffer. Absorbances at wavelengths of 490 and 520 nm were measured by fluorescence Elisa reader.

Detection of the loss of mitochondrial membrane potential

The loss of mitochondrial membrane potential was detected by JC-1 mitochondrial membrane potential kit (MitoPT JC-1, ImmunoChemistry Technologies, LLC). Cells (1×10^6) were seeded and treated with different concentrations of compounds. After, cells were incubated for 24 hours, they were collected by centrifugation at 1000 rpm for 10 minutes. Plate was read at 510 and 580 nm wavelengths by fluorescence Elisa reader. Ultimately, 585/510 values were calculated to determine the changes in mitochondrial membrane potential.

4.1.4. Statistical analysis

The data were reported as means±standard deviations and analysed by one-way analysis of variance (ANOVA) followed by the Tukey's multiple comparison tests using GraphPad Prism 5. Differences between means at $p < 0.05$ level were considered significant.

4.2. *In silico* studies

Co-crystal structure of c-ABL kinase domain in complex with imatinib was obtained from RCSB PDB (https://www.rcsb.org/) with 1IEP code. Schrödinger Protein Preparation Wizard was used to prepare protein. Water molecules were removed from proteins before docking calculations. Ligands were prepared as not charged by using Schrödinger LigPrep tool. Prepared ligands were docked into c-ABL kinase while DFG motif out position by using Schrödinger Glide-SP Flexible Docking procedure.

REFERENCES

[1] WHO report on cancer: setting priorities, investing wisely and providing care for all. World Health Organization, 2020. License: CC BY-NC-SA 3.0 IGO. https://apps.who.int/iris/handle/10665/330745, (accessed August 5, 2020).

[2] NIH National Cancer Institute. https://www.cancer.gov/types, (accessed August 5, 2020).

[3] Sun J, Wei Q, Zhou Y, Wang J, Liu Q, Xu H. A systematic analysis of FDA-approved anticancer drugs. BMC Syst Biol. 2017; 11(Suppl 5): 87. [CrossRef]

[4] Levitzki A. Tyrosine Kinase Inhibitors: Views of Selectivity, Sensitivity, and Clinical Performance. Annu Rev Pharmacol Toxicol. 2013; 53: 161-185.

[5] Schindler T, Bornmann W, Pellicena P, Miller WT, Clarkson B, Kuriyan J. Structural Mechanism for STI-571 Inhibition of Abelson Tyrosine Kinase. Science. 2000; 289(5486): 1938-1942.

[6] Roskoski R Jr. Properties of FDA-approved small molecule protein kinase inhibitors. Pharmacol Res. 2019; 144: 19-50. [CrossRef]

[7] Hanahan D, Weinberg RA. The hallmarks of cancer. Cell. 2000; 100(1): 57-70. [CrossRef]

[8] Bhullar KS, Lagarón NO, McGowan EM, Parmar I, Jha A, Hubbard BP, Rupasinghe HPV. Kinase-targeted cancer therapies: progress, challenges and future directions. Mol Cancer. 2018; 17: 48. [CrossRef]

[9] Cui JJ. A new challenging and promising era of tyrosine kinase inhibitors. ACS Med Chem Lett. 2014; 5(4): 272-274. [CrossRef]

[10] Nowell PC. Discovery of the Philadelphia chromosome : a personal perspective. J Clin Invest. 2007; 17(8): 2033-2035.

[11] Türe A, Kahraman DC, Cetin-Atalay R, Helvacıoğlu S, Charehsaz M, Küçükgüzel İ. Synthesis, anticancer activity, toxicity evaluation and molecular docking studies of novel phenylaminopyrimidine-(thio)urea hybrids as potential kinase inhibitors. Comput Biol Chem. 2019; 78: 227-241. [CrossRef]

[12] Türe A, Ergül M, Ergül M, Altun A, Küçükgüzel İ. Design, synthesis, and anticancer activity of novel 4-thiazolidinone-phenylaminopyrimidine hybrids. Mol Divers. 2020; 10.1007/s11030-020-10087-1. [CrossRef]

[13] Vermes I, Haanen C, Steffens-Nakken H, Reutelingsperger C. A novel assay for apoptosis. Flow cytometric detection of phosphatidylserine expression on early apoptotic cells using fluorescein labelled Annexin V. J Immunol Methods. 1995; 184(1): 39-51. [CrossRef]

[14] Boice A, Bouchier-Hayes L. Targeting apoptotic caspases in cancer. Biochim Biophys Acta Mol Cell Res. 2020; 1867(6): 118688. [CrossRef]

[15] Fiskum G, Kowaltowksi AJ, Andreyev AY, Kushnareva YE, Starkov AA. Apoptosis-related activities measured with isolated mitochondria and digitonin-permeabilized cells. Methods Enzymol. 2000; 322: 222-234. [CrossRef]

[16] Stevens M, Oltean S. Modulation of the Apoptosis Gene Bcl-x Function Through Alternative Splicing. Front Genet. 2019; 10: 804. [CrossRef]

[17] Escudier B, Eisen T, Stadler WM, et al. Sorafenib for treatment of renal cell carcinoma: Final efficacy and safety results of the phase III treatment approaches in renal cancer global evaluation trial. J Clin Oncol. 2009; 27(20): 3312-3318. [CrossRef]

[18] Woo HY, Heo J. Sorafenib in liver cancer. Expert Opin Pharmacother. 2012; 13(7): 1059-1067. [CrossRef]

[19] White PT, Cohen MS. The discovery and development of sorafenib for the treatment of thyroid cancer. Expert Opin Drug Discov. 2015; 10(4): 427-439. [CrossRef]

[20] Dietrich J, Hulme C, Hurley LH. The design, synthesis, and evaluation of 8 hybrid DFG-out allosteric kinase inhibitors: a structural analysis of the binding interactions of Gleevec, Nexavar, and BIRB-796. Bioorg Med Chem. 2010; 18(15): 5738-5748. [CrossRef]

[21] Shah P, Westwell AD. The role of fluorine in medicinal chemistry. J Enzyme Inhib Med Chem. 2007; 22(5): 527-540. [CrossRef]

[22] Druker BJ. Inhibition of the Bcr-Abl tyrosine kinase as a therapeutic strategy for CML. Oncogene. 2002; 21(56): 8541-8546. [CrossRef]

[23] Cortez D, Reuther G, Pendergast AM. The Bcr-Abl tyrosine kinase activates mitogenic signaling pathways and stimulates G1-to-S phase transition in hematopoietic cells. Onkogene. 1997; 15: 2333-2342.